JACS
JOURNAL OF THE AMERICAN CHEMICAL SOCIETY
pubs.acs.org/JACS

Article

Observation of Photophysical Processes of a Heptacene Derivative: Monomeric Behavior in Homogeneous Solution and Singlet Fission in Thin Film

Shinjiro Suzuki, Hayato Sakai, Mitsuaki Yamauchi, Hironobu Hayashi, Yoshiyuki Mizuhata, Tatsuhisa Kato, Takashi Hirose,* Taku Hasobe,* and Hiroko Yamada*

Cite This: J. Am. Chem. Soc. 2026, 148, 6000−6011

Read Online

ACCESS | Metrics & More | Article Recommendations | Supporting Information

ABSTRACT: A soluble heptacene derivative, 5,9,14,18-tetrakis-(triisopropylsilylethynyl)-heptacene (**TIPS-Hep**), was synthesized in situ from an α-diketone precursor via the Strating−Zwanenburg reaction, and its photophysical properties were comprehensively characterized in both solution and thin-film states. In deoxygenated dilute tetrahydrofuran (THF) solution, **TIPS-Hep** exhibited monomeric behavior. Absorption peaks were observed at 671, 737, 820, and 970 nm, accompanied by a shoulder at 870 nm, while fluorescence peaks were observed at 894 and 961 nm with a fluorescence lifetime (τ_S) of <100 ps. Nanosecond transient absorption spectroscopy revealed a triplet lifetime (τ_T) of 19 μs and a triplet quantum yield (Φ_{ISC}) of ∼2%. The short excited-state lifetime in dilute solution was estimated to be 87 ps by femtosecond transient absorption spectroscopy and precludes efficient molecular encounters, indicating that singlet fission is unlikely and that intersystem crossing serves as the dominant pathway for triplet formation. This interpretation is supported by transient decay analysis, which revealed no kinetic signatures associated with SF. In contrast, solution-processed thin films of **TIPS-Hep**, generated in situ by photoirradiation of a spin-coated α-diketone precursor, exhibited faster and enhanced formation of the triplet excited states. Since multiple excited species are involved, several kinetic models were examined, and a sequential model based on a SF pathway ($S_1 + S_0 \rightarrow TT \rightarrow 2T_1$) was identified as the most consistent with the experimental results. Global analysis of femtosecond transient absorption data with the sequential SF model assuming three species revealed high yields of correlated triplet pairs (TT, 75% at the maximum value of 100%) and independent triplets (T_1, 20% at the maximum value of 200%). These results provide valuable mechanistic insights into the excited-state dynamics of higher acenes.

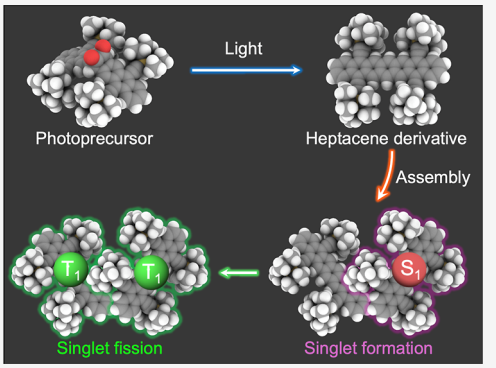

INTRODUCTION

Linearly fused higher acenes, especially those containing more than five benzene rings, have garnered significant interest due to their potential in near-infrared (NIR) optoelectronics and organic semiconductors.[1−6] Their distinct optical and electronic properties arise from extended π-conjugation and zigzag-edged structures, making them ideal model systems for exploring magnetism in carbon-based nanostructures. However, this same structural motif results in an exceptionally narrow highest occupied molecular orbital (HOMO)−lowest unoccupied molecular orbital (LUMO) gap with increasing acene length, compromising intrinsic stability. Moreover, the planar architecture and lack of solubilizing functional groups hinder their solubility, constraining their processability and device integration.

Among the synthetic strategies for higher acenes, the Strating−Zwanenburg reaction has proven to be particularly effective (Figure 1).[7] This visible-light-induced photodecarbonylation of α-diketones proceeds cleanly with gaseous byproducts, enabling the efficient formation of target acenes.[8−12] Using this approach, higher acenes have been accessed and characterized in matrices at cryogenic temperatures,[13,14] single crystals,[15] metal−organic frameworks,[16,17] and via on-surface synthesis under ultrahigh vacuum.[18−23] These advances have facilitated detailed investigations of their electronic structures. Thermal strategies have also been employed, including the cycloreversion of diheptacenes[24] and thermal decarbonylation of monoketone heptacene precursors,[25−28] though these typically require oxygen-free conditions.

Despite significant advances in understanding the photophysics of acenes less than pentacene,[1,29] the excited-state

Received: August 23, 2025
Revised: December 26, 2025
Accepted: January 21, 2026
Published: February 5, 2026

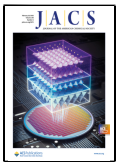

https://doi.org/10.1021/jacs.5c14689
J. Am. Chem. Soc. 2026, 148, 6000−6011

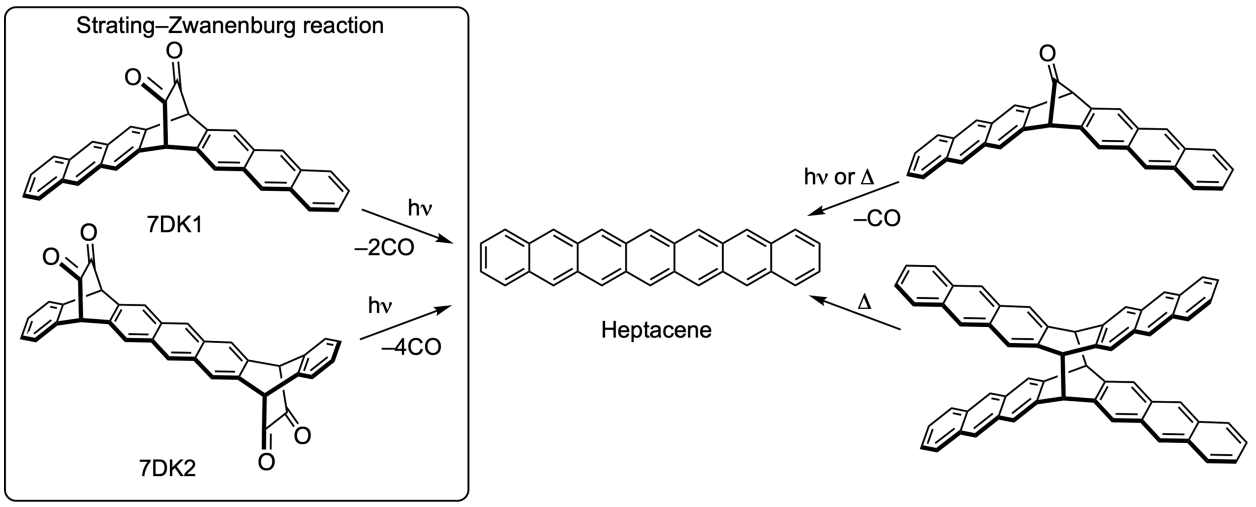

Figure 1. Synthesis of heptacene from photo- and thermal precursors.

behavior of pristine heptacene in solution at room temperature remains largely unexplored, primarily due to its extremely low solubility.[17,24,30−32] Its fluorescence spectrum in solution has, to date, eluded experimental observation, most likely due to its exceptionally low fluorescence quantum yield. This is consistent with spectroscopic and theoretical studies of up to hexacene, which reveal an acceleration of internal conversion with increasing acene length.[24,33] Recently, fluorescence from heptacene was detected at 77 K within a metal−organic framework (MOF) host using the photoprecursor, **7DK1**.[17] Neckers et al. successfully observed transient heptacene generated by nanosecond laser flash photolysis of **7DK1** in toluene, reporting the intersystem crossing (ISC) from the S_1 to T_1 state of heptacene with a lifetime of ∼7 ns, along with a triplet−triplet absorption at 580 nm decaying in 10.6 ± 0.1 μs.[13] The extremely low triplet energies of heptacene derivatives hinder the accurate determination of ISC quantum yields, and no Jablonski diagram with quantitatively determined quantum yields and rate constants for each process has yet been reported so far. While substituted heptacenes have been synthesized to improve solubility and stability,[30,32,34] comprehensive analyses of their excited-state dynamics remain absent.

Acenes are known to be excellent candidates for singlet fission (SF), where an excited singlet state (S_1) transfers energy to a neighboring ground-state molecule to form a correlated triplet pair (TT). SF has emerged as a promising route to boost photovoltaic efficiencies beyond the Shockley−Queisser limit (eq 1)[35−38]

$$S_0 + S_1 \rightarrow TT \rightarrow 2T_1 \quad (1)$$

Extensive studies on tetracene and pentacene have elucidated the SF mechanism, particularly when $E(S_1) \geq 2E(T_1)$.[39−58] Although SF was reported in hexacene derivatives ($E(S_1)$ = 1.8 eV, $E(T_1)$ = 0.4 eV),[59] experimental evidence for SF in heptacene remains absent. Theoretical predictions place $E(T_1)$ of heptacene between 0.24 and 0.69 eV,[60−62] with $E(S_1)$ around 1.54 eV.[59] The sufficient energy difference between $E(S_1)$ and 2 × $E(T_1)$ suggests that SF in heptacene is thermodynamically feasible. While the low $E(T_1)$ renders heptacene inefficient for photovoltaic applications, investigations of SF in heptacene and its derivatives offer valuable mechanistic insights into the excited-state dynamics of higher acenes.

Herein, we report the design, synthesis, and photophysical characterization of 5,9,14,18-tetrakis(triisopropylsilylethynyl)-heptacene (**TIPS-Hep**), achieving a long-sought advance in the photophysics of higher acenes through the stable observation of heptacene fluorescence in solution at room temperature. The strategic placement of four TIPS-ethynyl groups at previously unreported substitution sites not only ensures high solubility in solution but also affords a material that can be handled under deaerated conditions for detailed time-resolved studies in both solution and thin-film states. The synthetic accessibility of **TIPS-Hep** via the in situ Strating−Zwanenburg reaction (Scheme 1), its sufficient stability for the spectroscopic measurements, and its distinctive excited-state dynamics collectively position it as a valuable platform for unraveling the fundamental photophysics of higher acenes and advancing their application in optoelectronic devices.

Scheme 1. Photoconversion from TIPS-7DK to TIPS-Hep

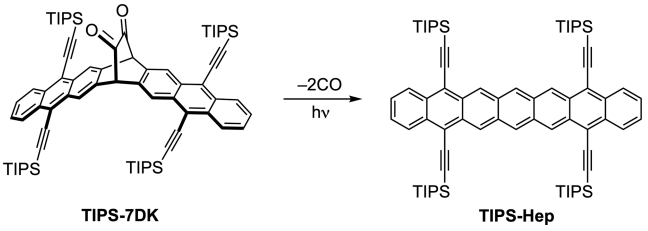

RESULTS AND DISCUSSION

The α-diketone precursor, **TIPS-7DK**, was synthesized as outlined in Scheme 2, beginning with the preparation of 1,4,5,8-tetrahydro-1,4:5,8-diepoxyanthracene (**1**) as a mixture of stereoisomers following the reported procedure.[63] Its reaction with 1,4-naphthoquinone in the presence of 3,6-di-2-pyridyl-1,2,4,5-tetrazine yielded a tetraone-diepoxy heptacene framework **2**. Insoluble stereoisomers were removed by filtration, and the filtrate was further converted to heptacene-5,9,14,18-tetraone (**3**). Subsequent ethynylation with lithium triisopropylsilylethyn-1-ide and methylation furnished compound **4**, which was transformed through a Diels−Alder reaction with vinylene carbonate, deoxygenative aromatization

https://doi.org/10.1021/jacs.5c14689
J. Am. Chem. Soc. 2026, 148, 6000−6011

Scheme 2. Synthetic Scheme of TIPS-7DK

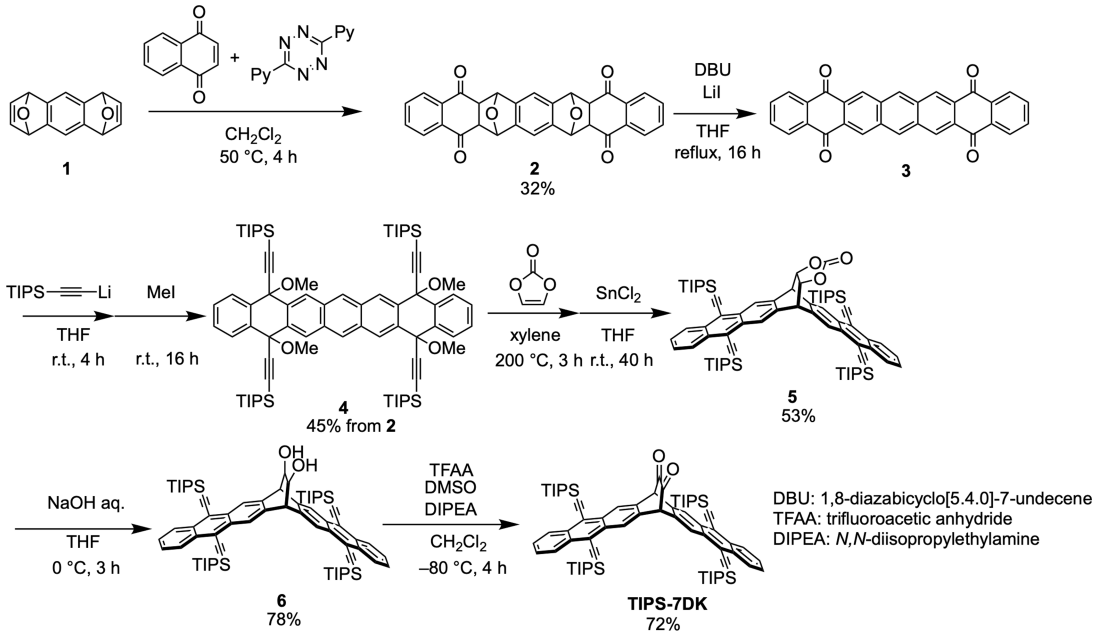

with $SnCl_2$, base-promoted hydrolysis, and Swern oxidation to the target α-diketone precursor, **TIPS-7DK**. Structures of intermediates were confirmed by ^1H and ^{13}C NMR spectroscopy and high-resolution mass spectrometry.

To generate **TIPS-Hep** for spectroscopic studies, **TIPS-7DK** was dissolved in a deoxygenated solvent inside a glovebox, using either an NMR sample tube or an optical cell equipped with a J. Young valve. The solution was then irradiated with a 470 nm LED light (400 mW cm^{-2}) for 20 min (Scheme 1). Complete conversion from **TIPS-7DK** to **TIPS-Hep** was confirmed by NMR spectroscopy (Figure S1a,b), with no detectable byproducts such as heptacene dimers. To measure the absorption spectrum of pure **TIPS-Hep** in $CDCl_3$, the solution was transferred to an optical cell, and the spectrum was recorded immediately following the NMR measurement (Figure S1c).

The evolution of the absorption spectrum during the photoconversion from **TIPS-7DK** to **TIPS-Hep** in THF is shown in Figure 2a–d. Upon photoirradiation, broad absorption band of α-diketone **TIPS-7DK** around 453 nm gradually diminished, while new peaks emerged at 671, 737, 820, and 970 nm, accompanied by a shoulder at 870 nm, indicating the formation of **TIPS-Hep**. It is noteworthy that the appearance of the weak absorption band at 970 nm is consistent with the feature previously reported for 6,8,15,17-tetrakis(triisopropylsilylethynyl)heptacene—an isomer of **TIPS-Hep** (6,8,15,17-**TIPS-Hep**) reported by Bunz et al.[31,32] Although the assignment of the weak band at 970 nm remains under discussion, it is most plausibly attributed to the symmetry-forbidden S_1 (^1A_g) ← S_0 transition.[24] The molar absorption coefficients of both **TIPS-7DK** and **TIPS-Hep** were determined in THF (Figure 2e,f). For reference, pristine heptacene—previously reported in 1-methylnaphthalene at 230 °C—exhibits absorption maxima at 623, 682, and 753 nm with a shoulder at 792 nm.[24] Compared to pristine heptacene, **TIPS-Hep** shows red-shifted absorption maxima by 50–70 nm, attributable to π-expansion through incorporation of the TIPS-ethynyl groups. Notably, the absorption spectrum of 6,8,15,17-**TIPS-Hep** in CH_2Cl_2 (10 μM) displays its most intense absorption at 865 nm, with a shoulder at 900 nm and a small peak at 1040 nm. The main peak is further red-shifted by 45 nm relative to **TIPS-Hep**.[31,32] These observations suggest that the electronic structure of **TIPS-Hep** more closely resembles that of pristine heptacene than that of the 6,8,15,17-TIPS-substituted isomer.

Heptacene has been reported to possess a biradical character in the ground state and readily undergoes dimerization in solution, particularly in the unsubstituted form.[24,64] To address the possibility of dimerization during the measurement, the absorbance at 820 nm was monitored at various concentrations. No significant spectral changes were observed up to 60 μM (Figure S2), and no evidence of dimer formation was detected within 300 s at 50 μM at ambient temperature (Figure S3a). When the solution was stored under an Ar atmosphere in the dark at ambient temperature for 24 h, the peaks at 671, 737, and 820 nm diminished by half, suggesting that slow dimerization occurs in the dark (Figure S3b,c). By normalization at 671 nm, the relative intensities at 671, 737, 820, 870, and 970 nm of the absorption spectra before and after 24 h remained unchanged, confirming that all these peaks originate from a single species, **TIPS-Hep** (Figure S3a). The change in the absorption spectrum of a **TIPS-Hep** solution at a higher concentration (200 μM) was monitored in the dark for 72 h (Figure S4). The absorption peaks of **TIPS-Hep** diminished and new peaks characteristic for shorter acenes increased. There are isosbestic points at 321, 420, 455, 486, 510, 525, and 553 nm. The change of ^1H NMR spectra of **TIPS-Hep** was also monitored at the same concentration (Figure S5). After 48 h, the formation of several byproducts was evident, characterized as several dimeric species by typical bridgehead proton signals at 6.13, 5.32, and 5.26 ppm.

The fluorescence spectra of **TIPS-Hep** in THF at room temperature exhibited emission peaks at 894 and 961 nm upon excitation at 820 nm (Figure 3a). By excitation at 350 nm, the fluorescence peaks were observed at the same wavelengths, and no emission was observed over 1000 nm (Figure S6). The relative fluorescence quantum yield (Φ_{FL}') was estimated as 0.020% using indocyanine green as a standard (Φ_{FL} = 5.1%)

https://doi.org/10.1021/jacs.5c14689
J. Am. Chem. Soc. 2026, 148, 6000–6011

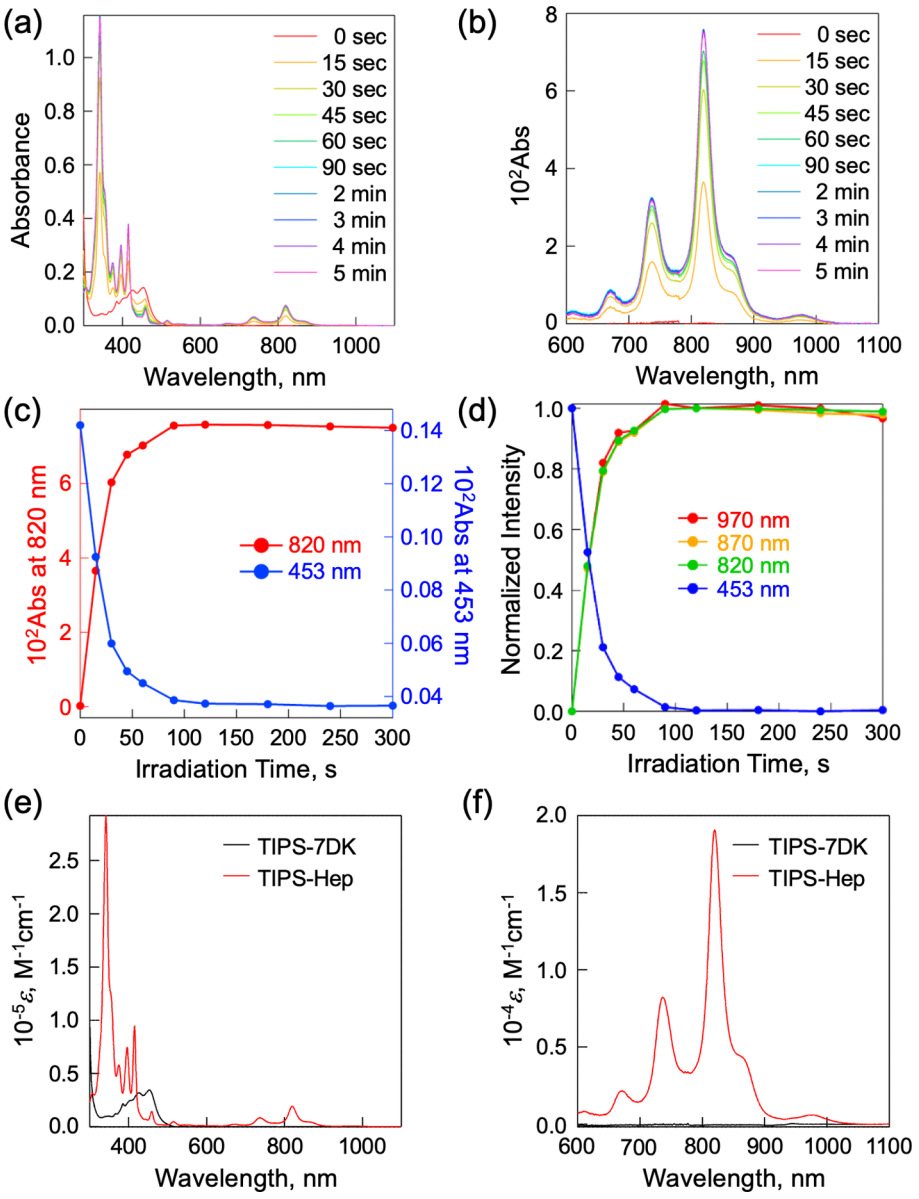

Figure 2. (a)Absorption spectral changes of **TIPS-7DK** in THF (50 μM) upon photoirradiation. (b) Magnified spectra in the 600−1100 nm region. Optical path length: 1 mm. (c) Time-dependent absorbance changes at 453 and 820 nm and (d) normalized time-dependent absorbance change at 453, 820, 870, and 970 nm during the photoconversion from **TIPS-7DK** to **TIPS-Hep**. (e) Molar absorption coefficients of **TIPS-7DK** and **TIPS-Hep** in THF. (f) Magnification (15 times) at 600−1100 nm.

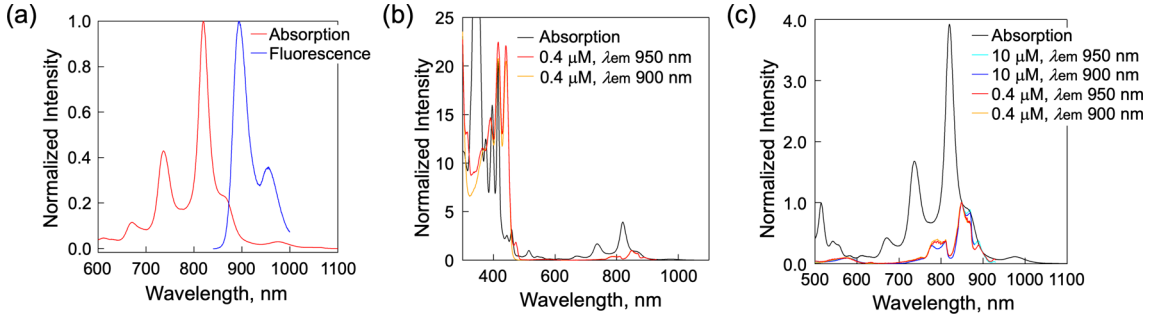

Figure 3. (a) Absorption (red) and fluorescence (blue, λ_{ex} = 820 nm) spectra of **TIPS-Hep** in THF (20 μM). Optical path length: 10 mm. (b,c) Normalized absorption and fluorescence excitation spectra (λ_{em} = 900 and 950 nm) of **TIPS-Hep** in THF. (b) 300−1100 nm region (0.4 μM). (c) 500−1100 nm region (0.4 and 10 μM).

(Figure S7 and Table S1).[17] The fluorescence lifetime (τ_{FL}') was measured to be less than 0.1 ns (20 μM, λ_{ex} = 820 nm, λ_{em} = 910 nm), limited by the instrument response function, suggesting a remarkably fast nonradiative decay rate (k_{nr}' > 1.1

https://doi.org/10.1021/jacs.5c14689
J. Am. Chem. Soc. 2026, 148, 6000−6011

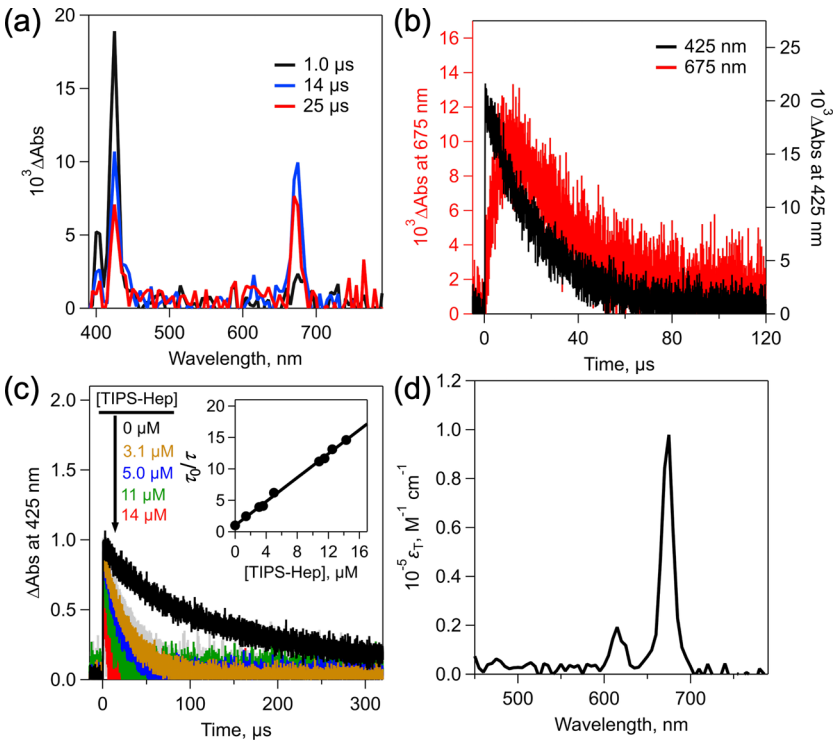

Figure 4. (a) Nanosecond transient absorption spectra (ns-TAS) of **Ant** (300 μM) in the presence of **TIPS-Hep** (5.0 μM) in THF. λ_{ex}: 355 nm. (b) The time profiles of **TIPS-Hep** (5.0 μM) in **Ant** solution (300 μM in THF) at 425 nm (black) and 675 nm (red). (c) The corresponding time-profiles of **Ant** (300 μM) at 425 nm in the presence of different concentrations of **TIPS-Hep** (0−14 μM). Absorbance at 425 nm was normalized at the initial absorbance. Inset: pseudo-first order plot of τ_0/τ monitored at 425 nm versus concentrations of **TIPS-Hep**. (d) The estimated ε_T values of **TIPS-Hep** in THF.

$\times 10^{10}$ s^{-1}) (Figure S8). The vibrational progression (ΔE) of the absorption and emission spectra were 1373 cm^{-1} (737−820 nm for absorption) and 780 cm^{-1} (894−961 nm for emission), respectively (Figure S9). The ΔE of the absorption bands were well reproduced by theoretical calculations at the RTD-CAM-B3LYP/6-31G(d) level using an adiabatic Hessian potential model (Figures S11−S13), whereas ΔE of the emission progression could not be reproduced by the same model.

Fluorescence excitation spectra were measured in THF by monitoring at 900 and 950 nm at the concentrations of 0.4 and 10 μM (Figure 3b,c). The peaks of the excitation spectra were observed around 800 and 860 nm, which are inconsistent with the main absorption bands at 737 and 820 nm. Due to the low sensitivity of the fluorescence excitation spectrum in the near-infrared region, the peak maxima cannot be determined precisely. Nevertheless, the ΔE between the bands at 860 and 800 nm is estimated to be ∼870 cm^{-1}, which is close to the ΔE of the emission peaks at 894 and 961 nm (∼780 cm^{-1}). These findings indicate that the fluorescence likely originates from the 870 nm shoulder, which is characteristic of heptacene derivatives.[31,32] The 870 nm absorption and corresponding 894/961 nm emission are therefore attributed to an electronic state in equilibrium with the ground state of **TIPS-Hep**. While the precise nature of this emissive species is not yet fully understood, similar shoulder absorption bands in extended acenes have often been discussed in the context of a singlet biradical form.[65,66] Consequently, the weak peak at 970 nm is attributed to the dipole-forbidden S_1 (2^1A_g) ← S_0 (1^1A_g) transition,[24,67] while the main absorption bands at 671, 737, and 820 nm correspond to the dipole-allowed S_2 (1^1B_{2u}) ← S_0 (1^1A_g) transition. Meanwhile, the weak shoulder around 870 nm is assigned to a transition associated with an alternative emissive state that exists in thermal equilibrium with the ground state. This interpretation rationalizes both the distinct vibronic spacings between absorption (∼1370 cm^{-1}) and emission (∼780 cm^{-1}) and the observation of emission from a higher-energy state (λ_{em} = 894 nm) relative to the lowest-energy absorption band (∼970 nm). While definitive experimental or computational evidence for the emissive species is not yet available, the consistency between the vibronic progressions of the excitation and emission spectra (∼780 cm^{-1}), strongly suggests that emissive state is in equilibrium with the ground state of **TIPS-Hep**.

To gain theoretical insights into the absorption and emission properties of **TIPS-Hep**, its optimized ground (S_0)-state geometry and excited states were calculated using time-dependent density functional theory (TD-DFT) and complete active space self-consistent field (CASSCF) methods. The excited-state calculations, based on the optimized S_0 geometry, employed the multireference CASSCF method, which is essential for describing dipole-forbidden excited states (^1A_g) that involve significant double excitation character.[17] As reference systems, calculations for pristine pentacene and heptacene at the CASSCF(6,6)/def2-SVP//RCAM-B3LYP-GD3BJ/6-31G(d) level reproduced the established inversion in the symmetry of their S_1 states: the S_1 state of pentacene is dipole-allowed ($^1B_{2u}$), whereas that of heptacene is dipole-forbidden (^1A_g), in agreement with previous theoretical studies (Table S2).[24,67] Building on this finding, we performed calculations at the same theoretical level for the TIPS-substituted analogues, 6,13-bis(triisopropylsilylethynyl)-

https://doi.org/10.1021/jacs.5c14689
J. Am. Chem. Soc. 2026, 148, 6000−6011

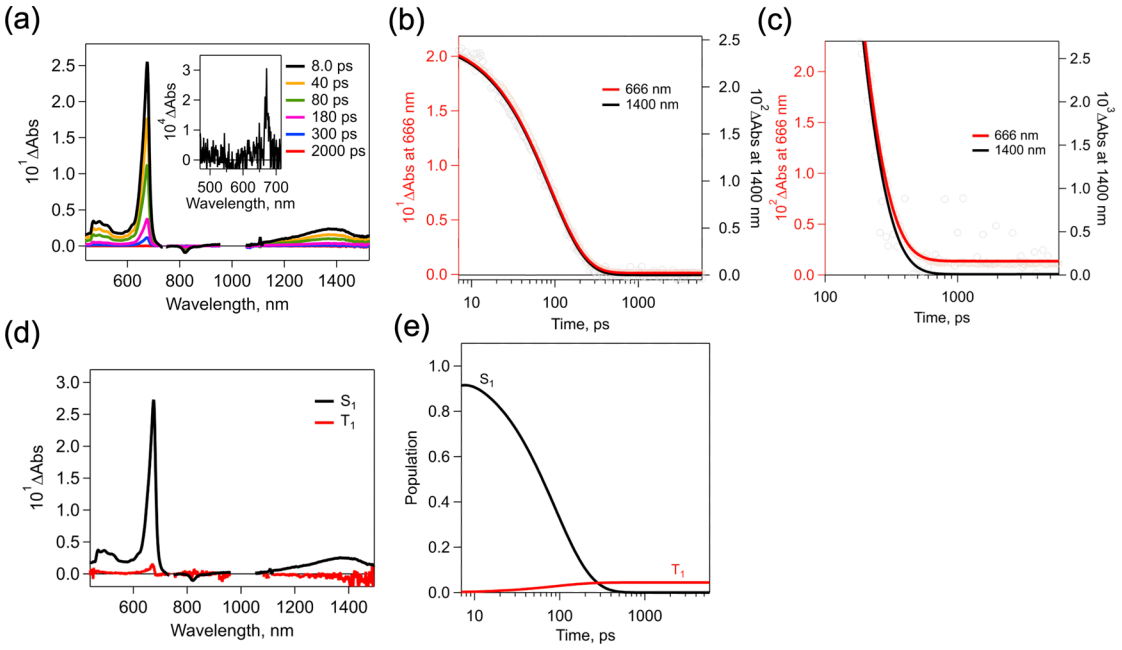

Figure 5. (a) Femtosecond transient absorption spectra (fs-TAS) of **TIPS-Hep** in THF (600 μM) irradiated at 740 nm, 0.64 μJ. Inset: an expansion of the spectrum at 2000 ps. (b) Time-profile at 666 (red) and 1400 (black) nm peaks and (c) magnification (10 times). (d) Species-associated spectra and (e) time-dependent population dynamics of S_1 and T_1 states.

pentacene (**TIPS-Pen**) and **TIPS-Hep**. The results revealed that the bulky TIPS-ethynyl groups do not alter the S_1-state ordering; notably, **TIPS-Hep** retains a dipole-forbidden S_1 state (^{1}Ag), indicating that its excited-state dynamics primary depend on the electronic structure of the heptacene backbone rather than by substituents. The diradical character (y_0) of pentacene, **TIPS-Pen**, heptacene, and **TIPS-Hep** were estimated as 0.378, 0.367, 0.629, and 0.810, respectively, suggesting significantly large diradical character (~81%) of **TIPS-Hep**.

Experimentally, the electron spin resonance (ESR) spectrum of **TIPS-Hep** at room temperature showed no detectable signal (Figure S10), in contrast to a previous report.[31] Consistent with this EPR-silent nature, the ^{1}H NMR spectrum of **TIPS-Hep** exhibited sharp resonances, indicating a lack of significant paramagnetic broadening. To gain deeper insight into the electronic structure, we performed theoretical calculations of **TIPS-Hep** at the UCAM-B3LYP/6-31G(d) level (Figures S14 and S15). Broken-symmetry (BS) DFT calculations revealed that the BS singlet state is more stable than the closed-shell singlet state by 30.1 kJ mol^{-1}. The resulting spin density is primarily localized along the zigzag edges of the heptacene core, that is typical for the higher acenes.

Furthermore, the optimized geometry of the BS state exhibits significantly reduced bond length alternation (BLA) compared to the closed-shell state, which is consistent with its high diradical character (Figure S15). These results, combined with the lack of an EPR signal, confirm that the ground state is a singlet (S = 0). This state is best described as a singlet diradicaloid rather than a traditional closed-shell molecule; the α and β spins are antiferromagnetically coupled, maintaining an EPR-silent singlet state while possessing significant diradical character.

To elucidate the triplet-state properties, measurements of nanosecond transient absorption spectra (ns-TAS) were performed on a 5.0 μM solution of **TIPS-Hep** in THF in the presence of 300 μM anthracene (**Ant**; a triplet sensitizer), upon excitation of **Ant** at 355 nm (Figure 4a). At 1 μs after excitation, a transient absorption (TA) peak at 425 nm, corresponding to the triplet state (T_1) of **Ant** (^{3}**Ant***), was observed. This signal decreased over time, while a new absorption band of **TIPS-Hep** at 675 nm, assignable to the T_1 state of **TIPS-Hep** sensitized via triplet−triplet energy transfer (TTET) from ^{3}**Ant***, gradually appeared. Kinetic analysis at 675 nm yielded a triplet lifetime (τ_T) of 19 μs (Figure 4b). Consistently, the decay profile at 425 nm indicated efficient quenching of ^{3}**Ant***, with a second-order rate constant for TTET from ^{3}**Ant*** to **TIPS-Hep** estimated as 4.8 × 10^9 M^{-1} s^{-1} (Figure 4c). This rate constant approaches the diffusion-controlled limit in THF (1.4 × 10^{10} M^{-1} s^{-1} at 298 K).[68] The triplet molar absorption coefficient (ε_T) of **TIPS-Hep** was estimated as 98,000 M^{-1} cm^{-1} at 675 nm (Figure 4d and Table S3), which was subsequently employed in the analysis of femtosecond transient absorption spectra (fs-TAS). Notably, the triplet signals from **TIPS-Hep** were not observed in the NIR region (ca. 1000−1500 nm) as described later in the fs-TAS measurements (Figure 5 and also see Figure S16).

The fs-TAS of a 600 μM THF solution of **TIPS-Hep** excited at 740 nm are shown in Figure 5a. Within 8.0 ps after photoexcitation, the TA bands attributed to the S_1 state of **TIPS-Hep** appeared in the 450−550 nm region with a vibronic structure, along with a sharp peak at 670 nm and 1100−1500 nm which decayed within 100 ps (Figure 5b). At 2000 ps, only a weak residual peak remained at 670 nm, which is assigned to the T_1 state of **TIPS-Hep** (Figure 5a). This result indicates that the peak at 670 nm includes contribution from both $S_1 \rightarrow S_n$ and $T_1 \rightarrow T_n$ transitions. Global analysis with a sequential model identified two species: the relaxed S_1 state and the T_1 state (Figure 5d,e). The lifetime of S_1 state (τ_S) was estimated to be 87 ps. As **TIPS-Hep** exists as monomers under these conditions, the T_1 state observed at 2000 ps is thought to originate from ISC from the S_1 state. We also evaluated the

https://doi.org/10.1021/jacs.5c14689
J. Am. Chem. Soc. 2026, 148, 6000−6011

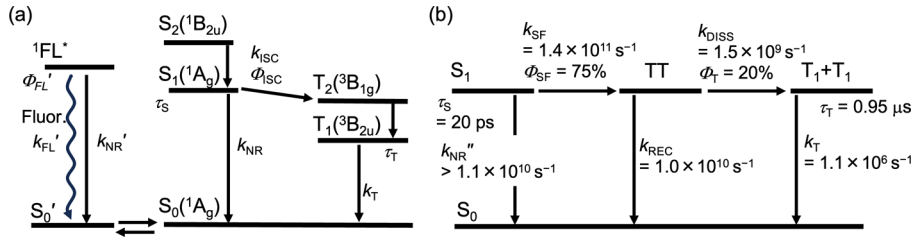

Figure 6. Kinetic models and corresponding photophysical parameters of **TIPS-Hep** (a) in THF and (b) in film. The parameters in (a) are summarized in Table 1. ^{1}FL*: the excited state of the emissive state. The k_{NR}' is derived from results obtained in THF solution and should be noted as an apparent value. In film, k_{NR}'' denotes the effective nonradiative decay constant, which includes both $S_1 \rightarrow S_0$ internal conversion and $S_1 \rightarrow T_1$ intersystem crossing. Since k_{ISC} is much smaller than k_{NR}, it can be considered negligible.

Table 1. Summarized Photophysical Properties of TIPS-Pen and TIPS-Hep.[a]

compd	solvent	k_{FL}'[b]/10^7 s^{-1} (Φ_{FL}'/%)	k_{NR}'[b]/10^{10} s^{-1} (Φ_{NR}'/%)	k_{FL}[d]/10^7 s^{-1} (Φ_{FL}/%)	k_{NR}[d]/10^{10} s^{-1} (Φ_{NR}/%)	k_{ISC}[d]/10^7 s^{-1} (Φ_{ISC}/%)	τ_S[e]/ns	τ_T[e]/μs
TIPS-Pen[f]	Me-THF	–	–	5.8[h] (75)[g]	0.00069[h] (9)[h]	1.2[h] (16)[f]	13[g]	24[f]
TIPS-Hep[i]	THF	>0.2 (>0.02)[c]	~1 (<99.98)	–	1.1[j] (97.6)[k]	28[j] (2.4)[k]	0.087[j]	10[j]

[a]Kinetic model of **TIPS-Hep** and **TIPS-Pen** in solution are shown in Figures 6a and S18, respectively. [b]Rate constants and quantum yields of the emissive state (S$_0$'), estimated assuming a thermal equilibrium between two ground-state species (S$_0$ and S$_0$'). The relative magnitudes of the rate constants are governed by this equilibrium. k_{FL}': fluorescence rate constant, defined as $k_{FL}' = \Phi_{FL}'/\tau_{FL}'$, where Φ_{FL}' is the fluorescence quantum yield and τ_{FL}' is the fluorescence lifetime. k_{NR}': nonradiative rate constant, defined as $k_{NR}' = (1-\Phi_{FL}')/\tau_{FL}'$. Φ_{NR}': quantum yield of internal conversion, defined as $\Phi_{NR}' = 1-\Phi_{FL}'$. [c]Because the absorptions of S$_0$ and S$_0$' overlap at the excitation wavelength (λ_{ex} = 740 nm), Φ_{FL}' represents a lower limit. [d]Rate constants and quantum yields of the ground state (S$_0$). k_{FL}: fluorescence rate constant, defined as $k_{FL} = \Phi_{FL}/\tau_{FL}$, where Φ_{FL} is the fluorescence quantum yield and τ_{FL} is the fluorescence lifetime. k_{NR}: nonradiative rate constant, defined as $k_{NR} = \Phi_{NR}/\tau_S$, where Φ_{NR} is the quantum yield of internal conversion, given by $\Phi_{NR} = 1-\Phi_{FL}-\Phi_{ISC}$. Φ_{ISC}: quantum yield of intersystem crossing, determined from ps-TAS measurements. [e]τ_S: lifetime of the singlet-excited state, defined as $\tau_S = 1/(k_{FL} + k_{NR} + k_{ISC})$. τ_T: lifetime of the triplet-excited state, defined as $\tau_T = 1/k_T$, where k_T is the decay constant of the triplet-excited state. [f]Reported value in Me-THF.[69] [g]Reported value in $CHCl_3$.[43] [h]Values estimated using the reported k_{FL}, Φ_{FL}, Φ_{ISC}, and τ_{S1} listed in this table. [i]This work. [j]According to target analysis, the uncertainty in the rate constants and lifetimes is approximately ±3%. [k]The standard deviations for ISC and NR are ±0.7%. See the SI for details of the calculations.

molar absorption coefficients of the S$_1$ state (ε_S) from the fs-TAS of **TIPS-Hep** (in THF) as described in Figures 5d and S16. The ε_S at 670 nm (1,400,000 M^{-1} cm^{-1}) is approximately 15 times larger than that of the corresponding ε_T (98,000 M^{-1} cm^{-1} at 675 nm). In THF, **TIPS-Hep** exhibits similar spectral shapes in both the S$_1$ and T$_1$ states across the visible range (500−700 nm), but the maximum ε_T value is at least 1 order of magnitude smaller than the ε_S value. In contrast, in the NIR region (ca. 1000−1500 nm), the TA of the S$_1$ state exhibits broad absorption bands, whereas that of the T$_1$ state falls below the detection limit due to the signal-to-noise ratio. The decay traces at 666 and 1400 nm (Figure 5b) exhibit highly consistent behavior up to approximately 300 ps. However, at 1000 ps, while the ΔAbs remains positive at 666 nm, it approaches zero at 1400 nm (Figures 5c). These observations suggest that the singlet-to-triplet conversion processes—such as ISC and SF, discussed later—should be carefully considered in terms of (i) the similarity of the TA spectral features between the S$_1$ and T$_1$ states and (ii) the remarkably intense S$_1$ signal. Additionally, excitation at 870 and 970 nm yielded the same results (Figures S17 and S18), indicating that the observed dynamics are independent of the excitation wavelength. As discussed earlier, the main singlet biradical ground state (S$_0$) and the emissive ground state (S$_0$') of **TIPS-Hep** exist in thermal equilibrium. The lack of excitation-wavelength dependence in the transient absorption spectra therefore suggests that the dynamics primarily originate from the singlet biradical species, which is more populated at equilibrium and intrinsically exhibits a stronger TA signal.

Separately, measurement of picosecond transient absorption spectra (ps-TAS) upon direct excitation of **TIPS-Hep** in THF (Figure S19) also revealed the triplet−triplet absorption through ISC process. Using the ε_T value estimated from ns-TAS (Figure 4d), the ISC quantum yield (Φ_{ISC}) was determined to be 2.4 ± 0.7% along with τ_T = ~ 10 μs. Based on the undetectable fluorescence from the S$_1$ state and Φ_{ISC} (~2%), the nonradiative quantum yield (Φ_{NR}) was approximately estimated to be ~98%. Consequently, the rate constants of ISC (k_{ISC}) and nonradiative decay (k_{NR}) were estimated to be 2.8 × 10^8 and 1.1 × 10^{10} s^{-1}, respectively (Figure 6a and Table 1).

The kinetic models and rate constants of **TIPS-Hep** are summarized in Figure 6a and Table 1, in comparison with **TIPS-Pen** (Figure S20), a benchmark acene derivative. According to previous reports, the values of k_{FL}, k_{NR}, and k_{ISC} of **TIPS-Pen** are 5.8 × 10^7, 6.9 × 10^6, and 1.2 × 10^7 s^{-1}, respectively (Table 1). In contrast, the values of k_{NR} and k_{ISC} for **TIPS-Hep** are 1.1 × 10^{10} and 2.8 × 10^8 s^{-1}, respectively, with a remarkably high Φ_{NR} of 98% (vide supra). The markedly different deactivation dynamics between **TIPS-Hep** and **TIPS-Pen**—namely, the absence of detectable emission from the S$_1$ state and the significantly enhanced nonradiative decay rates (k_{NR} and k_{ISC}) in **TIPS-Hep**—are indicative of the fundamentally distinct electronic nature of their S$_1$ states. **TIPS-Pen** exhibits prominent emission via the dipole-allowed S$_1$ (1^1B_{2u}) → S$_0$ (1^1A_g) transition (k_{FL} = 5.8 × 10^7 s^{-1}, Φ_{NR} = 75%), whereas **TIPS-Hep** shows no detectable emission from the S$_1$ state. The markedly enhanced nonradiative decay in **TIPS-Hep** is likely associated with a symmetry-allowed internal conversion from the dark S$_1$ (2^1A_g) state to the S$_0$ state (1^1A_g) of the same symmetry. Enhanced nonradiative decay with increasing numbers of annulated rings has also been observed for pristine acenes: the singlet lifetime (τ_S) of pentacene is 83 ns,[33] while that of heptacene is less than 7 ns.[13]

https://doi.org/10.1021/jacs.5c14689
J. Am. Chem. Soc. 2026, 148, 6000−6011

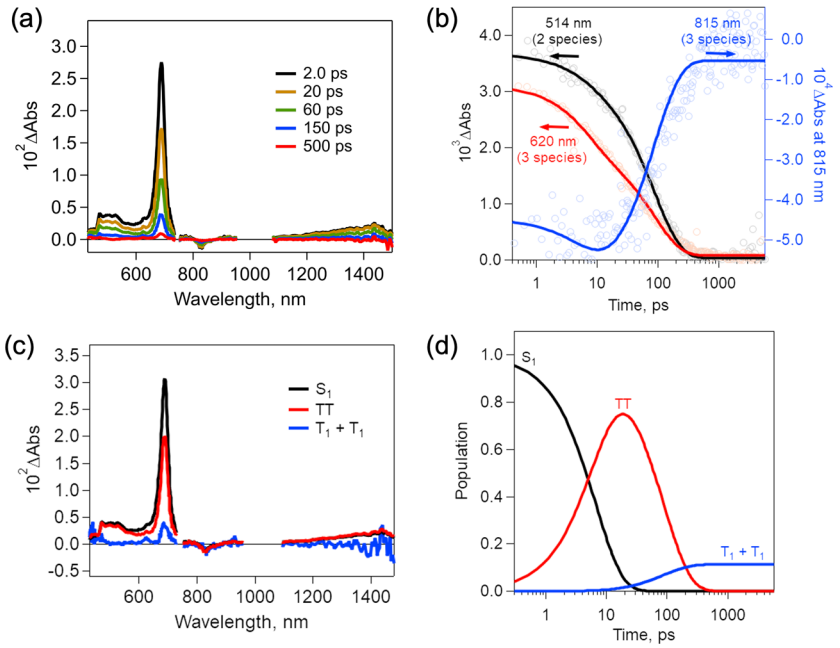

Figure 7. (a) Femtosecond transient absorption spectra (fs-TAS) of **TIPS-Hep** film under air irradiated at 740 nm, 0.70 μJ. (b) Fitting curves at 514, 620, and 815 nm after the irradiation obtained by the target analysis. (c) Species-associated spectra and (d) time-dependent population dynamics of S_1, TT, and $T_1 + T_1$ states.

In contrast to diluted solutions, where molecules are dispersed in isolation, bulk solids are expected to exhibit more complex excited-state dynamics involving multiple molecules as a result of intermolecular interactions. To investigate the excited-state dynamics of **TIPS-Hep** in the solid state, spin-coated films of **TIPS-Hep** were prepared from **TIPS-7DK** on quartz substrates and subsequently photo-irradiated with a 470 nm LED lamp for 1 h at 50 °C in a glovebox. The absorption spectra recorded before and after photoirradiation are shown in Figure S21. The absorption peaks are similar in shape to those observed in THF, with only slight wavelength shifts, indicating that **TIPS-Hep** does not undergo significant aggregation in the film state. This behavior contrasts with pristine heptacene, which has been reported to form aggregates in films and in single crystals, exhibiting broad absorption bands around 900 nm.[15,24] XRD measurements of the **TIPS-Hep** films on silicon (Si) substrates exhibited no diffraction peaks (Figure S22), consistent with an amorphous character. Although these substrates differ from quartz substrates used for the film fs-TAS measurements, both films exhibited similar appearance, suggesting that the quartz-based films are also amorphous character. Furthermore, AFM images on the Si-supported films revealed smooth film surfaces without notable grain boundaries or roughness (Figure S23), corroborating the absence of significant aggregation or crystallization upon spin-coating of **TIPS-7DK** and subsequent photoirradiation. Thus, the introduction of bulky TIPS-ethynyl substituents at the 5,9,14,18-positions of the heptacene backbone effectively suppresses strong intermolecular interactions which induce crystallization, dimerization or excimer formation in the film.

The fs-TAS measurements of the **TIPS-Hep** film under air (λ_{ex} = 740 nm) revealed an initial broad absorption spanning 450−550 and 1000−1500 nm, along with a sharp band at 690 nm, characteristic of the S_1 state absorption (Figure 7a and S24a). Over time, the broad features decayed while the 690 nm band persisted, which can be attributed to overlapping $S_1 \rightarrow S_n$ and $T_1 \rightarrow T_n$ transitions. The decay in Figure 7b and S24b show positive TA contributions mainly from the S_1 state at 514 nm, and from both S_1 and T_1 states at 620 nm, while a negative TA signal corresponding to ground-state bleaching (GSB) was observed at 815 nm. The sharp S_1 band exhibited a slight redshift from 670 nm in THF to 690 nm in the film, whereas the GSB shifted only marginally from 820 in THF to 815 nm in the film. The notable redshift in the solid state indicates intermolecular interactions among the **TIPS-Hep** molecules, despite the steric hindrance imposed by the bulky TIPS-ethynyl groups. The more pronounced redshift of the S_1 signal relative to the GSB suggests that these interactions are stronger in the S_1 state than in the ground state.

As demonstrated by the fs-TAS results in THF solution, the S_1 and T_1 spectra of **TIPS-Hep** are clearly distinguishable in the NIR region. In the thin-film fs-TAS measurements, transient absorption signals attributable to the S_1 state appeared immediately after photoexcitation at 740 nm, spanning 1000−1500 nm, and decayed with time. The time profiles at 514 and 620 nm exhibited two decay components, whereas that at 815 nm showed both a decay and a rise. The transient trace at 815 nm, corresponding to the GSB, is consistent with the global analysis model, although the relatively low signal-to-noise ratio in this NIR region precludes a definitive assignment of the subtle deepening observed in the first 10 ps. Although no further spectral evolution was observed after 300 ps, the ΔAbs values did not return to zero, suggesting that at least three excited species participate in the relaxation dynamics. Comparison of Figures 5 and 7 indicates that the decay of the S_1 state and the concomitant rise of the T_1 state are significantly accelerated in the solid state relative to the solution. This enhancement in triplet formation could arise from several possible pathways, including (i) accelerated intersystem crossing (ISC), (ii) symmetry-breaking charge separation (SBCS),[70,71] and (iii) singlet fission (SF). Among

https://doi.org/10.1021/jacs.5c14689
J. Am. Chem. Soc. 2026, 148, 6000−6011

these, the possibility of SBCS can be excluded, as no radical cation/anion signals characteristic of charge-separated species were detected in the fs-TAS spectra, unlike in previously reported systems.[72] Therefore, the accelerated triplet formation in the **TIPS-Hep** films is most likely attributed to enhanced ISC and/or SF processes.

To evaluate whether the sequential SF model provides an appropriate description of the excited-state dynamics, we compared it with three alternative kinetic models: (i) a three-component multiexponential fit, (ii) a model involving only ISC, and (iii) a model incorporating two competing ISC pathways (Figures S25−S27). In all these cases, the fitting curves were inconsistent with the experimentally observed time-dependent behaviors, and species-associated spectra (SAS) failed to reproduce physically reasonable features. Therefore, we conclude that the sequential SF model most accurately represents the excited state relaxation process in this system (Figure 7).

The global analysis (target analysis) using the sequential model (Figure 6b) provided three independent spectra of each S_1, TT, and $T_1 + T_1$ species (Figure 7c), and time-dependent population dynamics over time (Figure 7d). The three-component sequential relaxation process is different from the dynamics in solution (Figure 5), where only S_1 and T_1 were observed. The S_1 and $T_1 + T_1$ spectra closely resemble those of the S_1 and T_1 in THF, as described above. In contrast, the TT spectrum obtained from the global analysis exhibits a shape similar to that of S_1. Given the significant difference in molar absorption coefficients between singlet and triplet states, this resemblance can reasonably be similarity between the electronic states in the TT state and the S_1 state, which inevitably causes the TT spectrum to appear closer in shape to S_1. Another possible explanation is the presence of a heterogeneous molecular environment in the amorphous film (vide infra), where a small fraction of relatively long-lived S_1 state may persist.

The rate constants determined from the global analysis are as follows: nonradiative decay from S_1 to S_0 ($k_{NR}'' > 1.1 \times 10^{10}$ s^{-1}), singlet fission from S_1 to TT ($k_{SF} = 1.4 \times 10^{11}$ s^{-1}), TT dissociation to $T_1 + T_1$ ($k_{DISS} = 1.5 \times 10^{9}$ s^{-1}), and TT recombination to the ground state ($k_{REC} = 1.0 \times 10^{10}$ s^{-1}). Notably, k_{SF} (1.4×10^{11} s^{-1}) is about 3 orders of magnitude greater than k_{ISC} (2.8×10^{8} s^{-1}), indicating a substantial acceleration of the triplet formation in the thin film. Based on the population ratios such as S_1/TT and $S_1/(T_1 + T_1)$ from the target analysis, the quantum yields of TT and T_1 generation (Φ_{SF} and Φ_T) were estimated to be 75% and 20%, respectively (Figure 7d). Considering that the maximum Φ_{SF} and Φ_T values are 100% and 200%, respectively, these results certainly demonstrate the occurrence of SF. However, optimization of 'electronic coupling' and 'conformational flexibility' associated with molecular orientation is essential for further efficiency improvements.[73] The S_1 quenching rate constant in film (1.5×10^{11} s^{-1}) is also significantly faster than in solution (1.1×10^{10} s^{-1}), attributed to the SF process in the solid state. The XRD results indicated that the thin film was amorphous, suggesting that there were no strong interactions between **TIPS-Hep** molecules in the film.

Therefore, it was assumed that the molar absorption coefficient of **TIPS-Hep** was identical in the THF solution and in the thin film. We then calculated Φ_T using the following method. When the transient spectra in THF and thin film are normalized at the S_1 absorption maximum, the ΔAbs values at the T_1 maximum are 0.00133 in THF solution and 0.0109 in the film, respectively (Figure S28). Using the obtained triplet quantum yield (Φ_{ISC}) of **TIPS-Hep** in THF (2.4%) as a reference, the triplet quantum yield (Φ_T) in the film was estimated to be (0.0109/0.00133) × 2.4 = 20%. This value (20%) is quantitatively reliable, even considering that both monomer-like and aggregated species with slightly different decay may coexist within the amorphous film. It is also noteworthy that this value is an order of magnitude greater than Φ_{ISC} in THF (~2%), further supporting SF as the dominant triplet pathway.

Regarding the ISC, the amorphous nature of the film, as confirmed by XRD measurements, suggests that vibration suppression effects are minimal.[15,70] Despite Φ_{SF} = 75%, the Φ_T value (~20%) is relatively low, which may be due to the short lifetime of the TT state (20 ps), insufficient for spin conversion to yield two independent triplets. Taken together with the absorption and XRD results, these results indicate that the bulky TIPS-ethynyl substituents at the 5,9,14,18-positions effectively suppress strong aggregation of the heptacene backbones in the solid state. This steric hindrance not only prevents the formation of detrimental excimers or dimers (as observed in pristine heptacene) but also promotes a spatially isolated yet electronically coupled arrangement that facilitate SF from $S_1 + S_0$ to TT.

Based on these results, we conclude that SF occurs in the **TIPS-Hep** film. To further examine the excitation-wavelength dependent dynamics, fs-TAS measurements were performed at 870 and 970 nm (Figures S29 and S30). The results were consistent across all excitation wavelengths, indicating that SF proceeds after nearly quantitative internal conversion from S_2 to S_1. Even when the S_1 state was directly excited at 970 nm, SF proceeds with dynamics similar to those observed under S_2 excitation, except for the absence of $S_2 \rightarrow S_1$ relaxation.

To further investigate the long-lived triplet states, ps-TAS measurements of the **TIPS-Hep** film were conducted (Figure S31). The T_1 lifetime was determined to be ~0.95 μs ($k_T = 1.1 \times 10^6$ s^{-1}), significantly longer than those typically reported for acene films. This prolonged triplet lifetime is likely associated with the amorphous morphology discussed above. Moreover, no laser power dependence was observed in fs-TAS measurements between 0.45 to 3.45 μJ (Figure S32), supporting the amorphous nature of the film. The absence of laser-intensity-dependent quenching processes, such as singlet−singlet annihilation, further indicates that molecular orientation and aggregation are minimal in the **TIPS-Hep** film.

CONCLUSIONS

In this study, we successfully synthesized and characterized 5,9,14,18-tetrakis(triisopropylsilylethynyl)heptacene (**TIPS-Hep**), a soluble and stable heptacene derivative. Pure **TIPS-Hep** was obtained through an in situ Strating−Zwanenburg reaction from its α-diketone precursor (**TIPS-7DK**), enabling detailed photophysical analysis in both solution and thin-film states under ambient conditions.

In deoxygenated THF at room temperature, **TIPS-Hep** exhibited monomeric properties with a weak absorption peak at 970 nm attributed to the dipole-forbidden S_1 (2^1A_g) ← S_0 (1^1A_g) transition, the main absorption bands at 671, 737, and 820 nm to the dipole-allowed S_2 (1^1B_{2u}) ← S_0 (1^1A_g) transition, and the weak shoulder around 870 nm to an electronic state in equilibrium with the ground state of **TIPS-Hep**. The fluorescence peaks were observed at 894 and 961

https://doi.org/10.1021/jacs.5c14689
J. Am. Chem. Soc. 2026, 148, 6000−6011

nm with a low fluorescence quantum yield (Φ_{FL}' = 0.02%) and a short fluorescence lifetime (<100 ps). The consistency between the vibronic progressions of the excitation and emission spectra (~780 cm^{-1}) strongly suggests that the emissive state is in equilibrium with the ground state of **TIPS-Hep**. From the transient absorption measurements, ISC quantum yield (Φ_{ISC}) was estimated to be 2.4 ± 0.8% together with τ_T = ~ 10 μs, with triplet formation proceeding via internal conversion. The nonradiative decay from the S_1 energy was dominant and no singlet fission was observed in the solution phase.

Conversely, in spin-coated thin films, **TIPS-Hep** showed faster and enhanced formation of the triplet excited states. Since multiple excited species are involved in fs-TAS, several kinetic models were analyzed, and a sequential SF model was determined to be the most appropriate. The significantly enhanced S_1 quenching rate constant (5.1×10^{10} s^{-1}) and global analysis with a sequential model identified the formation of triplet pairs (TT) and free triplets (T_1) with respective yields of 75% and 20%. This is the first observation of singlet fission using heptacene as far as we know. Importantly, the bulky TIPS-ethynyl substituents at the 5,9,14,18-positions effectively suppress strong aggregation of the heptacene backbone in the solid state, thereby minimizing unproductive dimerization while still allowing the favorable intermolecular interactions necessary for efficient SF. These results enhance the understanding of photophysical processes in extended acenes. The study offers valuable guidelines for developing advanced organic electronic devices.

■ ASSOCIATED CONTENT

Supporting Information

The Supporting Information is available free of charge at https://pubs.acs.org/doi/10.1021/jacs.5c14689.

Materials, instrumentation, analytical methods, synthesis, additional analytical data, theoretical caculation, and additional characterization data (PDF)

■ AUTHOR INFORMATION

Corresponding Authors

Takashi Hirose − *Institute for Chemical Research, Kyoto University, Uji, Kyoto 611-0011, Japan;* orcid.org/0000-0002-5351-2101; Email: hirose@scl.kyoto-u.ac.jp

Taku Hasobe − *Department of Chemistry, Faculty of Science and Technology, Keio University, Yokohama, Kanagawa 223-8522, Japan;* orcid.org/0000-0002-4728-9767; Email: hasobe@chem.keio.ac.jp

Hiroko Yamada − *Institute for Chemical Research, Kyoto University, Uji, Kyoto 611-0011, Japan;* orcid.org/0000-0002-2138-5902; Email: hyamada@scl.kyoto-u.ac.jp

Authors

Shinjiro Suzuki − *Institute for Chemical Research, Kyoto University, Uji, Kyoto 611-0011, Japan*

Hayato Sakai − *Department of Chemistry, Faculty of Science and Technology, Keio University, Yokohama, Kanagawa 223-8522, Japan*

Mitsuaki Yamauchi − *Institute for Chemical Research, Kyoto University, Uji, Kyoto 611-0011, Japan;* orcid.org/0000-0003-0005-5960

Hironobu Hayashi − *Center for Basic Research on Materials, National Institute for Materials Science (NIMS), Tsukuba, Ibaraki 305-0047, Japan;* orcid.org/0000-0002-7872-3052

Yoshiyuki Mizuhata − *Institute for Chemical Research, Kyoto University, Uji, Kyoto 611-0011, Japan;* orcid.org/0000-0001-5301-0024

Tatsuhisa Kato − *Fukui Institute for Fundamental Chemistry, Kyoto University, Sakyo-ku, Kyoto 606-8103, Japan*

Complete contact information is available at: https://pubs.acs.org/10.1021/jacs.5c14689

Author Contributions

The manuscript was written through contributions of all authors. All authors have given approval to the final version of the manuscript.

Funding

This work was supported by Japan Society for the Promotion of Science (JSPS) KAKENHI (Grant Numbers JP25K01751 to H.Y., JP24K01473 to T.Hasobe, JP22K14556 to M.Y., and JP24K01576 to H.H.), the JSPS Bilateral Program (JPJSBP120243209 to H.Y.), Grant-in-Aids for Transformative Research Areas "Dynamic Exciton" (JP20H05833 to H.Y.) and "Material Science of Meso-Hierarchy" (JP23H04876 to T. Hasobe, JP24H01714 to M.Y., and JP24H01713 to T.Hirose), Nagase Science and Technology Foundation to H.Y., and Tokyo Ohka Foundation for The Promotion of Science and Technology to H.Y. Additional support was provided by the International Collaborative Research Program of Institute for Chemical Research (ICR), Kyoto University. This work was partially carried out through the joint research program of the Molecular Photoscience Research Center, Kobe University, and the Research Program of "Five-star Alliance" in "NJRC Mater. & Dev".

Notes

The authors declare no competing financial interest.

■ ACKNOWLEDGMENTS

The authors are grateful to Dr. Kengo Suzuki, Hiromi Suzuki, and Takahiro Miyazaki, Hamamatsu Photonics K.K. for the measurement of fluorescence lifetime. We also thank Dr. Nobutaka Shioya, Dr. Hiroshi Matsuda, Prof. Dr. Takeshi Hasegawa, Institute of Chemical Research (ICR), Kyoto University, for XRD measurements. Additional support was provided by the Joint Usage/Research Center [JURC, ICR, Kyoto University] by providing access to a Bruker Avance III 600 NMR spectrometer and a Bruker E500 spectrometer equipped with a super high Q resonator (ER 4122SHQ). We also acknowledge the SuperComputer System, ICR, Kyoto University for providing computation time.

■ ABBREVIATIONS

CH_2Cl_2	dichloromethane
LED	light emitting diode
TD-DFT	time-dependent density-functional theory
THF	tetrahydrofuran
TLC	thin layer chromatography.

■ REFERENCES

(1) Anthony, J. E. Functionalized Acenes and Heteroacenes for Organic Electronics. *Chem. Rev.* **2006**, *106*, 5028−5048.

(2) Watanabe, M.; Chen, K.-Y.; Chang, Y. J.; Chow, T. J. Acenes Generated from Precursors and Their Semiconducting Properties. *Acc. Chem. Res.* **2013**, *46*, 1606−1615.
(3) Suzuki, M.; Aotake, T.; Yamaguchi, Y.; Noguchi, N.; Nakano, H.; Nakayama, K.; Yamada, H. Synthesis and Photoreactivity of α-Diketone-Type Precursors of Acenes and Their Use in Organic-Device Fabrication. *J. Photochem. Photobiol. C: Photochem. Rev.* **2014**, *18*, 50−70.
(4) Yamada, H.; Kuzuhara, D.; Suzuki, M.; Hayashi, H.; Aratani, N. Synthesis and Morphological Control of Organic Semiconducting Materials Using the Precursor Approach. *Bull. Chem. Soc. Jpn.* **2020**, *93*, 1234−1267.
(5) Tönshoff, C.; Bettinger, H. F. Pushing the Limits of Acene Chemistry: The Recent Surge of Large Acenes. *Chem.—Eur. J.* **2021**, *27*, 3193−3212.
(6) Hayashi, H.; Yamada, H. Exploring the Chemistry of Higher Acenes: From Synthesis to Applications. *Chem. Sci.* **2025**, *16*, 11204−11231.
(7) Strating, J.; Zwanenburg, B.; Wagenaar, A.; Udding, A. C. Evidence for the Expulsion of Bis-CO from Bridged Alpha-Diketones. *Tetrahedron Lett.* **1969**, *10*, 125−128.
(8) Mondal, R.; Shah, B. K.; Neckers, D. C. Photogeneration of Heptacene in a Polymer Matrix. *J. Am. Chem. Soc.* **2006**, *128*, 9612−9613.
(9) Mondal, R.; Adhikari, R. M.; Shah, B. K.; Neckers, D. C. Revisiting the Stability of Hexacenes. *Org. Lett.* **2007**, *9*, 2505−2508.
(10) Mondal, R.; Tönshoff, C.; Khon, D.; Neckers, D. C.; Bettinger, H. F. Synthesis, Stability, and Photochemistry of Pentacene, Hexacene, and Heptacene: A Matrix Isolation Study. *J. Am. Chem. Soc.* **2009**, *131*, 14281−14289.
(11) Uno, H.; Yamashita, Y.; Kikuchi, M.; Watanabe, H.; Yamada, H.; Okujima, T.; Ogawa, T.; Ono, N. Photo Precursor for Pentacene. *Tetrahedron Lett.* **2005**, *46*, 1981−1983.
(12) Yamada, H.; Yamashita, Y.; Kikuchi, M.; Watanabe, H.; Okujima, T.; Uno, H.; Ogawa, T.; Ohara, K.; Ono, N. Photochemical Synthesis of Pentacene and Its Derivatives. *Chem.—Eur. J.* **2005**, *11*, 6212−6220.
(13) Mondal, R.; Okhrimenko, A. N.; Shah, B. K.; Neckers, D. C. Photodecarbonylation of α-Diketones: A Mechanistic Study of Reactions Leading to Acenes. *J. Phys. Chem. B* **2008**, *112*, 11−15.
(14) Tönshoff, C.; Bettinger, H. F. Photogeneration of Octacene and Nonacene. *Angew. Chem. Inter. Ed.* **2010**, *4*, 4125−4128.
(15) Hayashi, H.; Hieda, N.; Yamauchi, M.; Chan, Y. S.; Aratani, N.; Masuo, S.; Yamada, H. Visible-Light-Induced Heptacene Generation under Ambient Conditions: Utilization of Single-crystal Interior as an Isolated Reaction Site. *Chem.—Eur. J.* **2020**, *26*, 15079−15083.
(16) Kitao, T.; Miura, T.; Nakayama, R.; Tsutsui, Y.; Chan, Y. S.; Hayashi, H.; Yamada, H.; Seki, S.; Hitosugi, T.; Uemura, T. Synthesis of Polyacene by Using a Metal−Organic Framework. *Nat. Synth.* **2023**, *2*, 848−854.
(17) Miura, T.; Kitao, T.; Yamada, K. E.; Chan, Y. S.; Hayashi, H.; Yamada, H.; Uemura, T. Accessing Single-Molecule Properties of Heptacene Using a Metal-Organic Framework. *Chem.—Eur. J.* **2025**, *31*, No. e202501787.
(18) Urgel, J. I.; Hayashi, H.; Di Giovannantonio, M.; Pignedoli, C. A.; Mishra, S.; Deniz, O.; Yamashita, M.; Dienel, T.; Ruffieux, P.; Yamada, H.; Fasel, R. On-Surface Synthesis of Heptacene Organometallic Complexes. *J. Am. Chem. Soc.* **2017**, *139*, 11658−11661.
(19) Urgel, J. I.; Di Giovannantonio, M.; Gandus, G.; Chen, Q.; Liu, X.; Hayashi, H.; Ruffieux, P.; Decurtins, S.; Narita, A.; Passerone, D.; Yamada, H.; Liu, S.-X.; Müllen, K.; Pignedoli, C. A.; Fasel, R. Overcoming Steric Hindrance in Aryl-Aryl Homocoupling via On-Surface Copolymerization. *ChemPhysChem* **2019**, *20*, 2360−2366.
(20) Urgel, J. I.; Mishra, S.; Hayashi, H.; Wilhelm, J.; Pignedoli, C. A.; Di Giovannantonio, M.; Widmer, R.; Yamashita, M.; Hieda, N.; Ruffieux, P.; Yamada, H.; Fasel, R. On-Surface Light-Induced Generation of Higher Acenes and Elucidation of Their Open-Shell Character. *Nat. Commun.* **2019**, *10*, 861.
(21) Ayani, C. G.; Pisarra, M.; Urgel, J. I.; Navarro, J. J.; Díaz, C.; Hayashi, H.; Yamada, H.; Calleja, F.; Miranda, R.; Fasel, R.; Martín, F.; Vázquez de Parga, A. L. Efficient Photogeneration of Nonacene on Nanostructured Graphene. *Nanoscale Horiz.* **2021**, *6*, 744−750.
(22) Eimre, K.; Urgel, J. I.; Hayashi, H.; Di Giovannantonio, M.; Ruffieux, P.; Sato, S.; Otomo, S.; Chan, Y. S.; Aratani, N.; Passerone, D.; Gröning, O.; Yamada, H.; Fasel, R.; Pignedoli, C. A. On-Surface Synthesis and Characterization of Nitrogen-Substituted Undecacenes. *Nat. Commun.* **2022**, *13*, 511.
(23) Zugermeier, M.; Gruber, M.; Schmid, M.; Klein, B. P.; Ruppenthal, L.; Müller, P.; Einholz, R.; Hieringer, W.; Berndt, R.; Bettinger, H. F.; Gottfried, J. M. On-Surface Synthesis of Heptacene and Its Interaction with a Metal Surface. *Nanoscale* **2017**, *9*, 12461−12469.
(24) Einholz, R.; Fang, T.; Berger, R.; Grüninger, P.; Früh, A.; Chassé, T.; Fink, R. F.; Bettinger, H. F. H. Characterization in Solution, in the Solid State, and in Films. *J. Am. Chem. Soc.* **2017**, *139*, 4435−4442.
(25) Watanabe, M.; Chang, Y. J.; Liu, S.-W.; Chao, T.-H.; Goto, K.; Islam, M. M.; Yuan, C.-H.; Tao, Y.-T.; Shinmyozu, T.; Chow, T. J. The Synthesis, Crystal Structure and Charge-Transport Properties of Hexacene. *Nat. Chem.* **2012**, *4*, 574−578.
(26) Watanabe, M.; Su, W.-T.; Chen, K.-Y.; Chien, C.-T.; Chao, T.-H.; Chang, Y. J.; Liu, S.-W.; Chow, T. J. A Soluble Precursor of Hexacene and Its Application in Thin Film Transistors. *Chem. Commun.* **2013**, *49*, 2240−2242.
(27) Miyazaki, T.; Watanabe, M.; Matsushima, T.; Chien, C.; Adachi, C.; Sun, S.; Furuta, H.; Chow, T. J. Heptacene: Synthesis and Its Hole-Transfer Property in Stable Thin Films. *Chem.—Eur. J.* **2021**, *27*, 10677−10684.
(28) Jančařík, A.; Holec, J.; Nagata, Y.; Šámal, M.; Gourdon, A. Preparative-Scale Synthesis of Nonacene. *Nat. Commun.* **2022**, *13*, 223.
(29) Miyata, K.; Conrad-Burton, F. S.; Geyer, F. L.; Zhu, X.-Y. Triplet Pair States in Singlet Fission. *Chem. Rev.* **2019**, *119*, 4261−4292.
(30) Chun, D.; Cheng, Y.; Wudl, F. The Most Stable and Fully Characterized Functionalized Heptacene. *Angew. Chem. Inter. Ed.* **2008**, *120*, 8508−8513.
(31) Zeitter, N.; Hippchen, N.; Baur, P.; Unterreiner, T. V.; Rominger, F.; Freudenberg, J.; Bunz, U. H. F. Pentacene to Octacene: The Limit of Fourfold TIPS-Ethynylation. *Org. Mater.* **2024**, *06*, 12−17.
(32) Zong, W.; Hippchen, N.; Zeitter, N.; Maier, S.; Ludwig, P.; Rominger, F.; Freudenberg, J.; Bunz, U. H. F. Stabilizing Azaheptacenes. *J. Am. Chem. Soc.* **2024**, *146*, 5793−5798.
(33) Nijegorodov, N.; Ramachandran, V.; Winkoun, D. P. The Dependence of the Absorption and Fluorescence Parameters, the Intersystem Crossing and Internal Conversion Rate Constants on the Number of Rings in Polyacene Molecules. *Spectrochim. Acta Part A: Mol. Biomol. Spectrosc.* **1997**, *53*, 1813−1824.
(34) Payne, M. M.; Parkin, S. R.; Anthony, J. E. Functionalized Higher Acenes: Hexacene and Heptacene. *J. Am. Chem. Soc.* **2005**, *127*, 8028−8029.
(35) Shockley, W.; Queisser, H. J. Detailed Balance Limit of Efficiency of P-n Junction Solar Cells. *J. Appl. Phys.* **1961**, *32*, 510−519.
(36) Singh, S.; Jones, W. J.; Siebrand, W.; Stoicheff, B. P.; Schneider, W. G. Laser Generation of Excitons and Fluorescence in Anthracene Crystals. *J. Chem. Phys.* **1965**, *42*, 330−342.
(37) Geacintov, N.; Pope, M.; Vogel, F. Effect of Magnetic Field on the Fluorescence of Tetracene Crystals: Exciton Fission. *Phys. Rev. Lett.* **1969**, *22*, 593−596.
(38) Hanna, M. C.; Nozik, A. J. Solar Conversion Efficiency of Photovoltaic and Photoelectrolysis Cells with Carrier Multiplication Absorbers. *J. Appl. Phys.* **2006**, *100*, 074510.
(39) Jundt, C.; Klein, G.; Sipp, B.; Le Moigne, J.; Joucla, M.; Villaeys, A. A. Exciton Dynamics in Pentacene Thin Films Studied by Pump-Probe Spectroscopy. *Chem. Phys. Lett.* **1995**, *241*, 84−88.

https://doi.org/10.1021/jacs.5c14689
J. Am. Chem. Soc. 2026, 148, 6000−6011

(40) Thorsmølle, V. K.; Averitt, R. D.; Demsar, J.; Smith, D. L.; Tretiak, S.; Martin, R. L.; Chi, X.; Crone, B. K.; Ramirez, A. P.; Taylor, A. J. Morphology Effectively Controls Singlet-Triplet Exciton Relaxation and Charge Transport in Organic Semiconductors. *Phys. Rev. Lett.* **2009**, *102*, 017401.
(41) Thorsmølle, V. K.; Averitt, R. D.; Demsar, J.; Smith, D. L.; Tretiak, S.; Martin, R. L.; Chi, X.; Crone, B. K.; Ramirez, A. P.; Taylor, A. J. Photoexcited Carrier Relaxation Dynamics in Pentacene Probed by Ultrafast Optical Spectroscopy: Influence of Morphology on Relaxation Processes. *Phys. B: Condens. Matter* **2009**, *404*, 3127−3130.
(42) Zimmerman, P. M.; Zhang, Z.; Musgrave, C. B. Singlet Fission in Pentacene through Multi-Exciton Quantum States. *Nat. Chem.* **2010**, *2*, 648−652.
(43) Walker, B. J.; Musser, A. J.; Beljonne, D.; Friend, R. H. Singlet Exciton Fission in Solution. *Nat. Chem.* **2013**, *5*, 1019−1024.
(44) Wan, Y.; Guo, Z.; Zhu, T.; Yan, S.; Johnson, J.; Huang, L. Cooperative Singlet and Triplet Exciton Transport in Tetracene Crystals Visualized by Ultrafast Microscopy. *Nat. Chem.* **2015**, *7*, 785−792.
(45) Sanders, S. N.; Kumarasamy, E.; Pun, A. B.; Trinh, M. T.; Choi, B.; Xia, J.; Taffet, E. J.; Low, J. Z.; Miller, J. R.; Roy, X.; Zhu, X.-Y.; Steigerwald, M. L.; Sfeir, M. Y.; Campos, L. M. Quantitative Intramolecular Singlet Fission in Bipentacenes. *J. Am. Chem. Soc.* **2015**, *137*, 8965−8972.
(46) Grieco, C.; Doucette, G. S.; Pensack, R. D.; Payne, M. M.; Rimshaw, A.; Scholes, G. D.; Anthony, J. E.; Asbury, J. B. Dynamic Exchange During Triplet Transport in Nanocrystalline TIPS-Pentacene Films. *J. Am. Chem. Soc.* **2016**, *138*, 16069−16080.
(47) Hetzer, C.; Guldi, D. M.; Tykwinski, R. R. Pentacene Dimers as a Critical Tool for the Investigation of Intramolecular Singlet Fission. *Chem.—Eur. J.* **2018**, *24*, 8245−8257.
(48) Wang, C.; Tauber, M. J. High-Yield Singlet Fission in a Zeaxanthin Aggregate Observed by Picosecond Resonance Raman Spectroscopy. *J. Am. Chem. Soc.* **2010**, *132*, 13988−13991.
(49) Johnson, J. C.; Nozik, A. J.; Michl, J. High Triplet Yield from Singlet Fission in a Thin Film of 1,3-Diphenylisobenzofuran. *J. Am. Chem. Soc.* **2010**, *132*, 16302−16303.
(50) Hartnett, P. E.; Margulies, E. A.; Mauck, C. M.; Miller, S. A.; Wu, Y.; Wu, Y.-L.; Marks, T. J.; Wasielewski, M. R. Effects of Crystal Morphology on Singlet Exciton Fission in Diketopyrrolopyrrole Thin Films. *J. Phys. Chem. B* **2016**, *120*, 1357−1366.
(51) Miyata, K.; Kurashige, Y.; Watanabe, K.; Sugimoto, T.; Takahashi, S.; Tanaka, S.; Takeya, J.; Yanai, T.; Matsumoto, Y. Coherent Singlet Fission Activated by Symmetry Breaking. *Nat. Chem.* **2017**, *9*, 983−989.
(52) Margulies, E. A.; Logsdon, J. L.; Miller, C. E.; Ma, L.; Simonoff, E.; Young, R. M.; Schatz, G. C.; Wasielewski, M. R. Direct Observation of a Charge-Transfer State Preceding High-Yield Singlet Fission in Terrylenediimide Thin Films. *J. Am. Chem. Soc.* **2017**, *139*, 663−671.
(53) Miller, C. E.; Wasielewski, M. R.; Schatz, G. C. Modeling Singlet Fission in Rylene and Diketopyrrolopyrrole Derivatives: The Role of the Charge Transfer State in Superexchange and Excimer Formation. *J. Phys. Chem. C* **2017**, *121*, 10345−10350.
(54) Eaton, S. W.; Shoer, L. E.; Karlen, S. D.; Dyar, S. M.; Margulies, E. A.; Veldkamp, B. S.; Ramanan, C.; Hartzler, D. A.; Savikhin, S.; Marks, T. J.; Wasielewski, M. R. Singlet Exciton Fission in Polycrystalline Thin Films of a Slip-Stacked Perylenediimide. *J. Am. Chem. Soc.* **2013**, *135*, 14701−14712.
(55) Musser, A. J.; Maiuri, M.; Brida, D.; Cerullo, G.; Friend, R. H.; Clark, J. The Nature of Singlet Exciton Fission in Carotenoid Aggregates. *J. Am. Chem. Soc.* **2015**, *137*, 5130−5139.
(56) Chan, W.-L.; Ligges, M.; Jailaubekov, A.; Kaake, L.; Miaja-Avila, L.; Zhu, X.-Y. Observing the Multiexciton State in Singlet Fission and Ensuing Ultrafast Multielectron Transfer. *Science* **2011**, *334*, 1541−1545.
(57) McGlynn, S. P.; Azumi, T.; Kasha, M. External Heavy-Atom Spin—Orbital Coupling Effect. V. Absorption Studies of Triplet States. *J. Chem. Phys.* **1964**, *40*, 507−515.
(58) Geacintov, N. E.; Burgos, J.; Pope, M.; Strom, C. Heterofission of Pentacene Excited Singlets in Pentacene-Doped Tetracene Crystals. *Chem. Phys. Lett.* **1971**, *11*, 504−508.
(59) Monahan, N. R.; Sun, D.; Tamura, H.; Williams, K. W.; Xu, B.; Zhong, Y.; Kumar, B.; Nuckolls, C.; Harutyunyan, A. R.; Chen, G.; Dai, H.-L.; Beljonne, D.; Rao, Y.; Zhu, X.-Y. Dynamics of the Triplet-Pair State Reveals the Likely Coexistence of Coherent and Incoherent Singlet Fission in Crystalline Hexacene. *Nat. Chem.* **2017**, *9*, 341−346.
(60) Houk, K. N.; Lee, P. S.; Nendel, M. Polyacene and Cyclacene Geometries and Electronic Structures: Bond Equalization, Vanishing Band Gaps, and Triplet Ground States Contrast with Polyacetylene. *J. Org. Chem.* **2001**, *66*, 5517−5521.
(61) Hajgató, B.; Szieberth, D.; Geerlings, P.; De Proft, F.; Deleuze, M. S. A Benchmark Theoretical Study of the Electronic Ground State and of the Singlet-Triplet Split of Benzene and Linear Acenes. *J. Chem. Phys.* **2009**, *131*, 224321.
(62) Chakraborty, H.; Shukla, A. Theory of Triplet Optical Absorption in Oligoacenes: From Naphthalene to Heptacene. *J. Chem. Phys.* **2014**, *141*, 164301.
(63) Shahlai, K.; Acquaah, S. O.; Hart, H. USE OF 1,2,4,5-TETRABROMOBENZENE AS A 1,4-BENZADIYNE EQUIVALENT: Anti- AND Syn-1,4,5,8-TETRAHYDROANTHRACENE 1,4:5,8-DIEPOXIDES. *Org. Synth.* **1998**, *75*, 201−205.
(64) Wagner, M. S.; Peisert, H.; Chassé, T.; Bettinger, H. F. Detection of Diheptacendiyl Diradical Intermediate in the Cycloreversion of Diheptacene to Heptacene. *Chem. Commun.* **2024**, *60*, 8451−8453.
(65) Zeitter, N.; Hippchen, N.; Maier, S.; Rominger, F.; Dreuw, A.; Freudenberg, J.; Bunz, U. H. F. Persistent Ambipolar Heptacenes and Their Redox Species. *Angew. Chem., Int. Ed.* **2022**, *61*, No. e202200918.
(66) Jousselin-Oba, T.; Mamada, M.; Wright, K.; Marrot, J.; Adachi, C.; Yassar, A.; Frigoli, M. Synthesis, Aromaticity, and Application of peri-Pentacenopentacene: Localized Representation of Benzenoid Aromatic Compounds. *Angew. Chem., Int. Ed.* **2022**, *61*, No. e202112794.
(67) Yang, Y.; Davidson, E. R.; Yang, W. Nature of Ground and Electronic Excited States of Higher Acenes. *Proc. Natl. Acad. Sci. U. S. A.* **2016**, *113*, E5098−E5107.
(68) Montalti, M.; Credi, A.; Prodi, L.; Gandolfi, M. T. *Handbook of Photochemistry* 3rd Ed.; CRC Press, 2020.
(69) Zirzlmeier, J.; Lehnherr, D.; Coto, P. B.; Chernick, E. T.; Casillas, R.; Basel, B. S.; Thoss, M.; Tykwinski, R. R.; Guldi, D. M. Singlet Fission in Pentacene Dimers. *Proc. Natl. Acad. Sci. U. S. A.* **2015**, *112*, 5325−5330.
(70) Lin, C.; Kim, T.; Schultz, J. D.; Young, R. M.; Wasielewski, M. R. Accelerating Symmetry-Breaking Charge Separation in a Perylenediimide Trimer through a Vibronically Coherent Dimer Intermediate. *Nat. Chem.* **2022**, *14*, 786−793.
(71) Young, R. M.; Wasielewski, M. R. Mixed Electronic States in Molecular Dimers: Connecting Singlet Fission, Excimer Formation, and Symmetry-Breaking Charge Transfer. *Acc. Chem. Res.* **2020**, *53*, 1957−1968.
(72) Bettinger, H. F.; Mondal, R.; Neckers, D. C. Stable Photoinduced Charge Separation in Heptacene. *Chem. Commun.* **2007**, 5209−5211.
(73) Hasobe, T.; Nakamura, S.; Tkachenko, N. V.; Kobori, Y. Molecular Design Strategy for High-Yield and Long-Lived Individual Doubled Triplet Excitons through Intramolecular Singlet Fissionplet-Excitons-through-Intramolecular.Pdf. *ACS Energy Lett.* **2022**, *7*, 390−400.

https://doi.org/10.1021/jacs.5c14689
J. Am. Chem. Soc. 2026, 148, 6000−6011